Progress In Electromagnetics Research M, Vol. 102, 127–135, 2021

Triple-Band Highly Efficient Multi-Polarization Converter Based on Reflective Metasurface

Lili Yuan, Lei Hou, and Zhengping Zhang*

Abstract—In this paper, a triple-band reflective polarization converter with high efficiency for both linear-to-linear and linear-to-circular polarizations based on a metasurface is proposed, which can rotate a linearly polarized (LP) incident wave into its orthogonal direction with over 90% polarization conversion ratio (PCR) in the bands of 5.5–5.9 GHz (relative bandwidth of 7%) and 12–17.7 GHz (relative bandwidth of 38.4%). Besides, the proposed converter can also transform a linearly polarized incident wave to circularly polarized (CP) wave in the band of 6–12 GHz (relative bandwidth of 66.7%). Additionally, the performance of proposed polarization converter stays in considerable stability with the incident angle increasing 60° in circular polarization and 30° in linear polarization. Moreover, the physical mechanism of multiple resonances is discussed based on surface current distributions and equivalent circuit model. A prototype of the proposed converter is fabricated and measured, and the experiments and simulations are in great agreement. This polarization converter can be employed to manipulate the polarization of the signal in microwave communication.

1. INTRODUCTION

Polarization is one of the inherent properties of electromagnetic (EM) waves [1, 2]. The polarization of EM wave refers to the oscillating direction of an electric field in propagation [3]. Polarization converters, for their special properties in polarization manipulation, have been applied a lot in microwave [4–8], terahertz [9, 10], and even optical frequencies [8, 11, 12]. Traditional polarization converters for manipulating polarization states usually employ optical activity crystals and polymers, which have the shortcomings of high profile and bulky volumes [13, 14]. Therefore, they are difficult to integrate into the device. Artificial EM polarization manipulation metasurfaces are one of the artificial materials that manipulate EM polarization properties, which can achieve electromagnetic properties that natural materials cannot achieve, thus, they can provide unprecedented opportunities to manipulate EM characteristics, including polarization [15–19].

Due to the numerous advantages of metasurfaces, many scholars have studied them. Li et al. designed a cross-polarization converter whose average PCR is greater than 90% for normal incident linearly polarized waves over a frequency range of 8.2–23 GHz, and they employed simulated surface current distributions to further analyze physical mechanisms [20]. Unit cells employing a square and L-shaped patches have been used to enhance polarization rotation bandwidth and polarization conversion ratio. Moreover, with the incident angle increasing from 0 to 60°, the 3-dB bandwidth of reflection coefficient r_{xy} is only reduced by about 2 GHz [21]. Zhao and Cheng used a cut-wire structure to acquire three resonances generated by electric and magnetic fields of incident wave, which could lead to bandwidth expansion extremely from 5.1 to 12.1 GHz [6]. Huang et al. presented a metasurface based on a concentric rectangular arrangement to achieve dual-band linear polarization whose r_{yx} over 0.8 was obtained in two frequency bands 4.35–5.05 GHz and 9.88–13.2 GHz [22]. Khan et al.

Received 27 March 2021, Accepted 27 April 2021, Scheduled 4 May 2021
* Corresponding author: Zhengping Zhang (zpzhang@gzu.edu.cn).
The authors are with College of Big Data and Information Engineering, Guizhou University, Guiyang 550025, China.

proposed a design which can completely pass a y-polarized wave as an x-polarized wave in the forward direction [23]. Zheng et al. proposed a dual-broadband reflective polarization converter which can achieve linear polarization in the lower frequency band of 7.74–14.44 GHz and circular polarization in the higher frequency band of 14.95–17.35 GHz [7]. Bakal et al. designed a new type of hybrid composite to improve radar absorbtion capability, and it can used in radar applications [24]. Yang et al. proposed a tri-band artificial electromagnetic polarization metasurface, which employed the equivalent circuit and surface current distribution to explain the polarization conversion physical mechanism [25]. Zheng et al. employed unit cells of two meander lines and one cut wire to transform a linearly polarized incident EM wave into its orthogonal LP reflection wave from 6.53 to 12.07 GHz with the PCR of 88% and a circularly polarized reflection wave from 13.7 to 15.6 GHz with a relative bandwidth of 13% [8]. Al-Badri et al. [26] and Sağık [27] proposed a dual band metamaterial perfect absorber for Ku band application and a type of metamaterial to improve the gain and directivity of microstrip patch antenna. Above all, multi-broadband and highly efficient polarization converter which simultaneously function for multi-polarizations are still worth studying.

In this paper, we propose a triple-band metasurface reflector constructed by a quarter circle with a triangular cone and a curved patch rotated 45°, which can rotate linearly polarized incident wave into its orthogonal direction with over 90% PCR in 5.5–5.9 GHz and 12–17.7 GHz, and transform linearly polarized incident wave to circularly polarized wave in the band of 6–11.6 GHz simultaneously. Additionally, the performance of proposed polarization converter stays in considerable stability with incident angle increasing 60° and 30° in achieving circular polarization and linear polarization, respectively.

2. ANALYSIS OF THE PROPOSED UNIT CELL

Schematic of the unit cell of the proposed polarization converter is depicted in Figure 1. It is composed of a top metallic copper structure and a metallic ground plate separated by a dielectric substrate layer. The top metallic structure is composed of a quarter circle with a triangular cone and a curved patch rotating 45° along $+y$-axis. The middle substrate is the F4B with a dielectric constant of 2.65, dielectric loss tangent of 0.002, and thickness $t = 2\,\text{mm}$. The metasurface formed by the periodic array of a cell with a symmetric structure can be treated as an anisotropic homogeneous material with dispersive relative permittivity and permeability. When a plane wave with a prescribed polarization illuminates the metasurface, both x- and y-polarized reflected waves are generated due to the anisotropic characteristics of the metasurface. The unit cell of the polarization converter is simulated and calculated by using finite element method, in which we set a Floquet port in the $+z$ direction with wave vector along the $-z$ direction and Master/Slave boundaries in $+x/-x$ and $+y/-y$ directions, respectively. Final parameters of the geometry are shown as follows: $p = 8\,\text{mm}$, $L1 = 7.8\,\text{mm}$, $L2 = 3\,\text{mm}$, $R1 = 5\,\text{mm}$, $R2 = 3.5\,\text{mm}$.

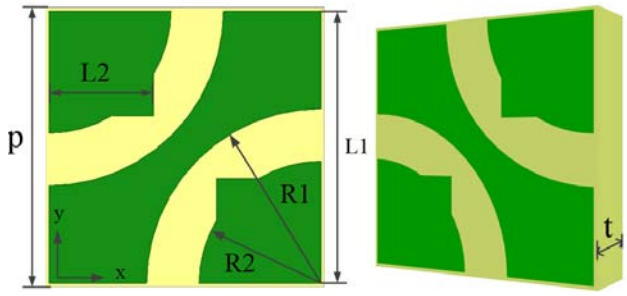

Figure 1. Schematic view of the unit cell.

Taking a y-polarized incident wave as an example, the reflected wave consists of both y- and x-polarized components:

$$\vec{E}^r_{\text{total}} = \vec{E}^r_x + \vec{E}^r_y = \vec{x} r_{xy} \left|\vec{E}^r_y\right| e^{-j(kz+\phi_{xy})} + \vec{y} r_{yy} \left|\vec{E}^r_y\right| e^{-j(kz+\phi_{yy})} \tag{1}$$

where $r_{xy} = \left|\vec{E}_x^r\right| / \left|\vec{E}_y^i\right|$ and $r_{yy} = \left|\vec{E}_y^r\right| / \left|\vec{E}_y^i\right|$ represent the reflection ratio of y-to-x (cross-polarization) and y-to-y polarization conversion (co-polarization), and ϕ_{xy} and ϕ_{yy} are the corresponding phases. PCR is defined as PCR $= r_{xy}^2/(r_{xy}^2 + r_{yy}^2)$ to evaluate the efficiency of cross-polarization conversion, and the AR is defined as:

$$\text{AR} = \left(\left(r_{xy}^2 + r_{yy}^2 + \sqrt{a}\right) / \left(r_{xy}^2 + r_{yy}^2 - \sqrt{a}\right)\right)^{1/2} \tag{2}$$

where $a = r_{xy}^4 + r_{yy}^4 + 2r_{xy}^2 r_{yy}^2 \cos(2\Delta\phi_{xy})$, the AR is employed to characterize the bandwidth of the LP to CP. The simulated reflection coefficients of co-polarization (r_{yy}) and cross-polarization (r_{xy}) are presented in Figure 2(a). It can be seen that r_{xy} is over 3-dB from 5.3 to 6.6 GHz and from 9.8 to 18.3 GHz. Three resonances occur at 5.8, 13.4, and 17.2 GHz. As shown in Figure 2(b), the structure achieves over 90% PCR in the lower band of 5.5–5.9 GHz and the higher band of 12–17.7 GHz with

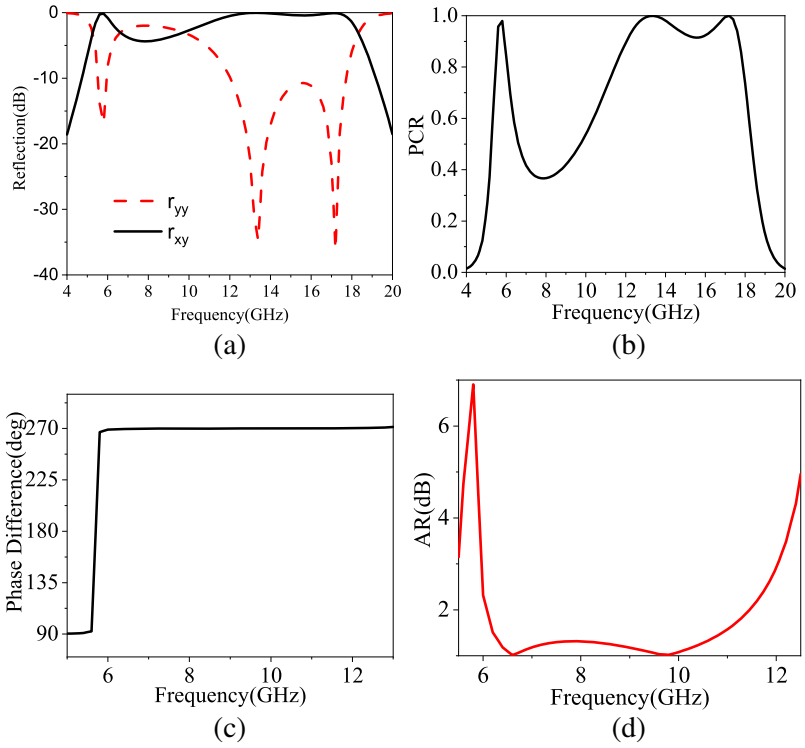

Figure 2. The polarization converter performance: (a) Co- and cross-polarized reflection coefficients, (b) PCR, (c) phase difference, (d) AR.

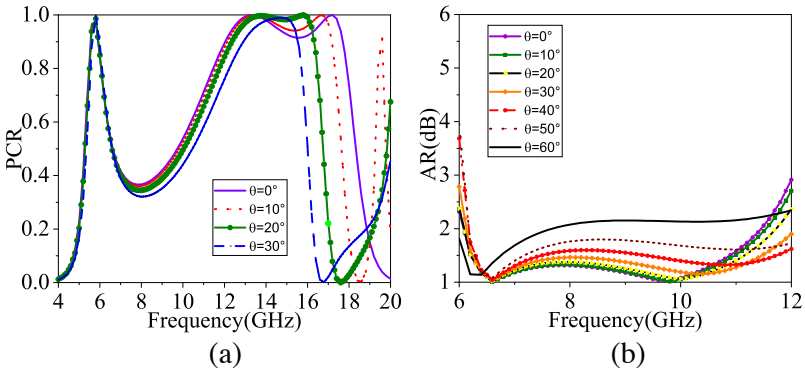

Figure 3. The polarization converter performance with different incident angles: (a) PCR, (b) AR.

a normal incident angle wave, where nearly 100% PCR can be achieved at three resonances. This phenomenon indicates that most energy of the y-polarized wave is rotated to the x-polarized one after being reflected by the metasurface. Figure 2(c) depicts the phase difference $\Delta\phi = \phi_{xy} - \phi_{yy}$, which is 270° in the band of 6–12 GHz. Without a doubt, it is very consistent with the phase difference required for line-to-circular polarization. The AR values are shown in Figure 2(d), in which AR is less than 3 dB from 6 to 12 GHz, which indicates that the proposed metasurface can transform linearly polarized incident wave to circularly polarized wave in the band of 6–12 GHz. To analyze the influence of oblique incidence in more details, we simulated the PCR and AR at different incident angles, respectively. As shown in Figure 3(a), we can conclude that when the incident angle (θ) changes from 0° to 30°, the PCR stays still over 0.9, except for a slight variation in the high frequency region. As shown in Figure 3(b), the AR remains stable, only a little overstep 3 dB at low frequencies as the incident angle increases. In summary, the proposed metasurface keeps an excellent polarization conversion characteristic in the oblique incidence.

3. THEORETICAL ANALYSIS

When the metasurface is illuminated by plane waves, both x- and y-polarized reflected waves are generated due to the anisotropic characteristics of the metasurface. Hence, the y-polarized incident EM wave ($\vec{E}_y^i$) can be decomposed into two perpendicular equal components along the u-axis ($\vec{E}_u^i$) and v-axis ($\vec{E}_v^i$), which are ±45° rotated with respect to the $+y$-axis, as shown in Figure 4(a). Thus, the incident EM wave can be expressed as follows:

$$\vec{E}_y^i = \vec{y}E_o e^{jkz} = \vec{E}_u^i + \vec{E}_v^i = \vec{u}\left|\vec{E}_u^i\right| e^{jkz} + \vec{v}\left|\vec{E}_v^i\right| e^{jkz} \tag{3}$$

where $\left|\vec{E}_u^i\right| = \left|\vec{E}_v^i\right| = (\sqrt{2}/2)E_o$. The reflection coefficients along the u- and v-axes can be written as r_u and r_v, so the reflected EM wave can be expressed as:

$$\vec{E}^r = \vec{E}_u^r + \vec{E}_v^r = \vec{u}r_u\left|\vec{E}_u^i\right| e^{j(kz+\phi_u)} + \vec{v}r_v\left|\vec{E}_v^i\right| e^{j(kz+\phi_v)} \tag{4}$$

when the reflection coefficients $r_u = r_v = r$ and phase difference $|\phi_u - \phi_v| = \pi$, we get:

$$\vec{E}^r = (\sqrt{2}/2)rE_o e^{j(kz+\phi_v)}(\vec{u}e^{j\pi} + \vec{v}) \tag{5}$$

when the reflection coefficients $r_u = r_v = r$ and phase difference $|\phi_u - \phi_v| = \pi/2$, we get:

$$\vec{E}^r = (\sqrt{2}/2)rE_o e^{j(kz+\phi_v)}(\vec{u}e^{j\pi/2} + \vec{v}) \tag{6}$$

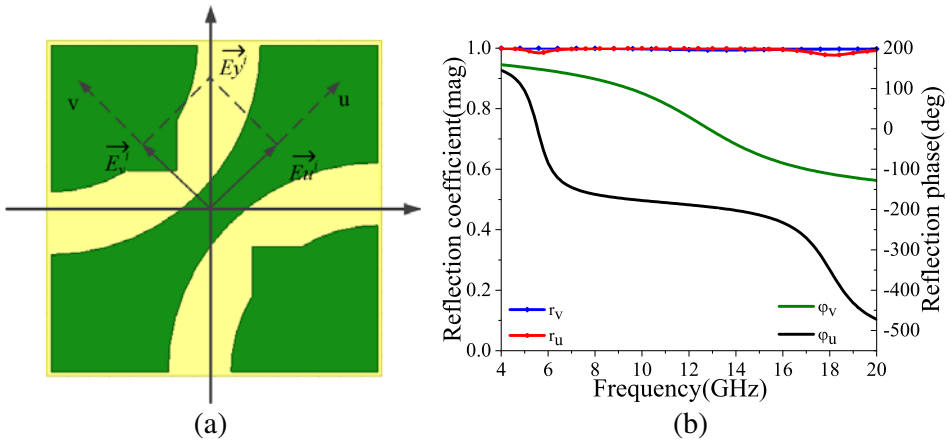

Figure 4. Electric field decomposition diagram: (a) u- and v-axis coordinate system, (b) reflection coefficients and phases for u- and v-polarization.

Apparently, when Equations (5) and (6) hold, LP-to-LP polarization conversion and LP-to-CP polarization conversion are obtained, respectively. In order to further study reflection coefficients, we combine the surface current distributions at three resonances for analysis. Figure 5 depicts the current distributions on the top metal patch and the metal ground of a unit cell under u-polarized and v-polarized incident waves, respectively.

When the metasurface is illuminated by v-polarized incident wave $\vec{E}_v^i$, the induced current distribution on the unit cell of patch along the v-axis is weak, as shown in Figures 5(f), 5(g), and 5(h). Thus, the proposed metasurface is equivalent to a same thickness dielectric layer with a metal ground, and the reflection amplitude coefficient and reflection phase are unaffected by the anisotropic metal patch. As shown in Figure 4(b), the amplitude coefficient $r_v \approx 1$, which is caused by the fact that the loss of dielectric material is quite small. In another situation, the induced current distributions on the metal patch and ground sheet under u-polarized incident wave $\vec{E}_u^i$ are shown in Figures 5(b), 5(c), and 5(d). The induced current distributions on the metal patch are always opposite to the induced current distributions on the metal ground sheet which results in magnetic resonator.

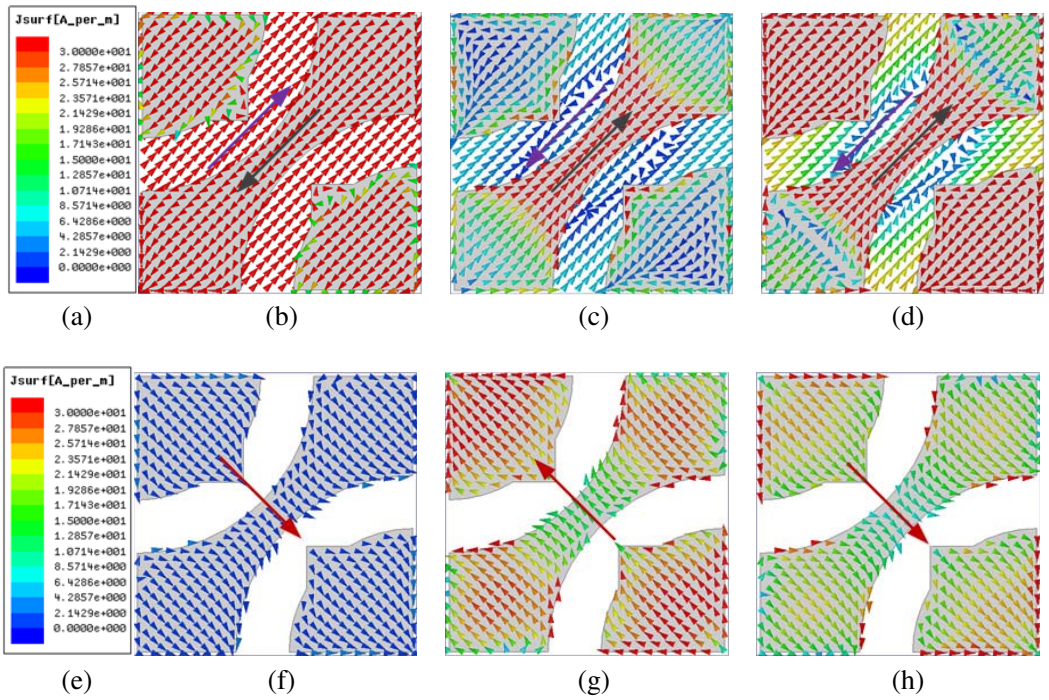

Figure 5. The induced current distributions under E_{iu} and E_{iv} at (b), (f) 5.8 GHz; (c), (g) 13.4 GHz; (d), (h) 17.2 GHz; (a) and (e) is label.

To further explain physical mechanism, an equivalent circuit of the proposed polarization converter is investigated, as shown in Figure 6(b). For the equivalent circuit, it is assumed that the gap between adjacent metal patches provides capacitances, and the metal patch is equivalent to an inductor. The gap between top metal structure and the bottom reflectance surface is equivalent to the capacitance, as shown in Figure 6(a). The Advanced Design System (ADS) is utilized to the simulation to obtain the parameter values of the lumped elements. By modeling and simulating the equivalent circuit in ADS, the values of inductance and capacitance are as follows: $L_1 = 0.29\,\text{nH}$, $L_2 = 0.28\,\text{nH}$, $L_3 = 0.12\,\text{nH}$, $L_4 = 1.17\,\text{nH}$, $L_5 = 4.19\,\text{nH}$, $L_6 = 0.24\,\text{nH}$, $C_1 = 0.3\,\text{pF}$, $C_2 = 4.56\,\text{pF}$, $C_3 = 1.13\,\text{pF}$, $C_4 = 0.38\,\text{pF}$, $C_5 = 4.8\,\text{pF}$, $C_6 = 0.57\,\text{pF}$. Based on these optimized parameters, the reflection coefficients of the equivalent circuit are calculated and compared, as shown in Figure 6(c). The curves calculated by HFSS and ADS are basically the same, and the discrepancies are mainly because of two reasons. Firstly, the results by ADS are only based on fundamental Floquet modes, while the results by HFSS include all coupling effects. Secondly, the equivalent circuit is just used to approximately calculate the S-parameters.

4. MEASUREMENT

A prototype consisting of 30 × 30 unit cells with a total dimension of 240 mm × 240 mm × 2 mm was fabricated and measured to validate the proposed design performance. The prototype and schematic view of the measurement setup are depicted in Figures 7(a) and (b). In the first step, two wideband horn antennas connected with a network analyzer are placed along the same direction for transmitting and receiving signals, respectively. In the second step, the receiving antenna is rotated with 90° to measure cross-polarization component. Then, the PCR and AR can be calculated using the measured results. It is worth noting that the measured results are calibrated with an equal-sized metallic plate. Figures 8(a), (b), and (c) show the comparison of the measured results and simulated ones. It can be indicated that the measurement and simulation results are in a reasonable agreement. The discrepancy mainly comes from two aspects. In an ideal state, the transmitting antenna and receiving antenna are not in the same position. According to Snell's law, the angle of 3–6° between the transmitting antenna and receiving antenna can make the antenna better receive and transmit EM waves. Therefore, there are discrepancies between the actual measurement results and simulation results obtained under the ideal state. The other is caused by the tolerance used in the fabrication.

Comparisons with other polarization converters based on metasurface are shown in Table 1. It can be concluded that previous converters are lack of the characteristics of multi-functions, and most of them can only achieve LP-to-LP or LP-to-CP. Moreover, the previous designed converters can achieve broadband performance with bulky volume. As expected, the proposed ultra-thin metasurface can achieve triple-band and high-efficient performance.

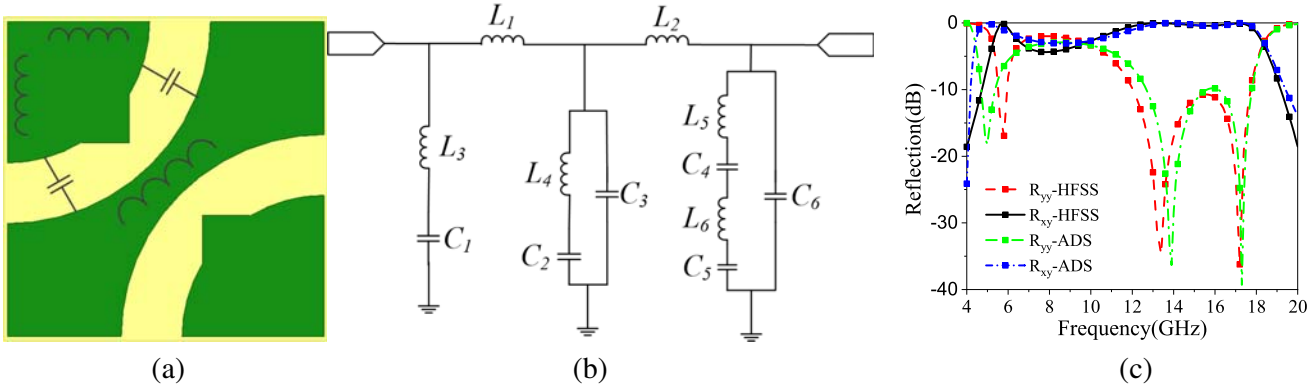

Figure 6. Equivalent circuit of the proposed polarization converter: (a) Analysis diagram of the equivalent circuit, (b) equivalent circuit model, (c) results simulated by ADS and HFSS.

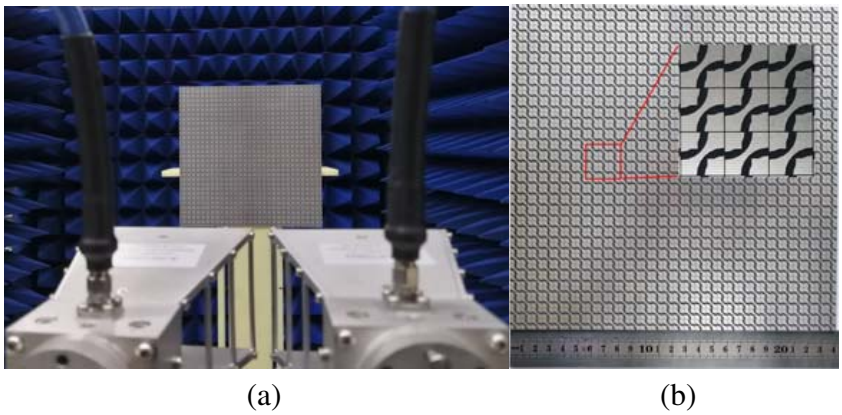

Figure 7. (a) Measurement environment, (b) fabricated sample.

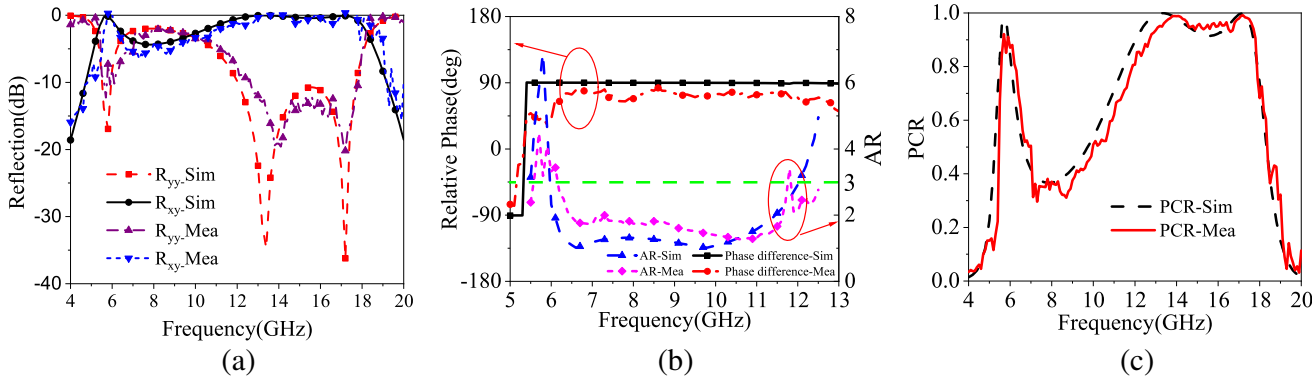

Figure 8. Simulated and measured results under normal incidence: (a) Reflection coefficients, (b) phase difference and AR, (c) PCR.

Table 1. Comparison of polarization converters.

Refs.	CF (GHz)	Thickness	Performance	FBW (%)	PCR	AR
Ref. [1]	15.7	4 mm	LP-to-CP	30.3	/	< 3 dB
Ref. [2]	14.37	2.5 mm	LP-to-LP	82.3	$> 90\%$	/
Ref. [7]	11.09	3 mm	LP-to-LP	60.4	$> 90\%$	/
	16.15		LP-to-CP	14.9	/	< 3 dB
Ref. [8]	9.3	3.1 mm	LP-to-LP	59.6	$> 88\%$	/
	14.65		LP-to-CP	13	/	< 3 dB
Ref. [22]	4.85, 11.525	2 mm	LP-to-LP	18.6, 36	$> 86\%$	/
This Work	5.7, 14.85	2 mm	LP-to-LP	7, 38.4	$> 90\%$	/
	8.8		LP-to-CP	63.6	/	< 3 dB

5. CONCLUSION

In this paper, a simple structure triple-broadband reflective polarization converter with high efficiency based on a metasurface is presented to convert the LP incident EM into its orthogonal LP reflection wave in two bands and a CP reflection wave in a band simultaneously. The simulation results demonstrate that the proposed metasurface can convert a y/x-polarized incident wave to an x/y-polarized one in 5.5–5.9 GHz and 12–17.7 GHz with over 90% PCR. Moreover, the metasurface can also convert an LP incident wave into a circular one in 6–12 GHz below 3 dB AR, which can be applied in C-band, X-band, and Ku-band of microwave communication. In addition, the proposed metasurface keeps an excellent polarization conversion characteristic in the oblique incidence. Surface current distributions and equivalent circuit are employed to explain the physical mechanism. Moreover, the simulation performance is validated by the prototype. Owing to its advantages of simple design and scalable geometry, the proposed design has potential application in polarization manipulation devices and antenna design.

ACKNOWLEDGMENT

This work was supported by the Guizhou University Talent Fund Cooperation (2019) No. 37.

REFERENCES

1. Zhang, Z., X. Cao, and L. Sijia, "Broadband metamaterial reflectors for polarization manipulation based on cross/ring resonators," *Radioengineering*, Vol. 25, No. 3, 436–441, 2016.
2. Zheng, Q., C. Guo, P. Yuan, Y.-H. Ren, and J. Ding, "Wideband and high-efficiency reflective polarization conversion metasurface based on anisotropic metamaterials," *J. Electron. Mater.*, Vol. 47, No. 5, 2658–2666, 2018.
3. Beruete, M., M. Navarro-Cía, M. Sorolla, and I. Campillo, "Polarization selection with stacked hole array metamaterial," *J. Appl. Phys.*, Vol. 103, No. 5, 1–5, 2008.
4. Xu, P., S.-Y. Wang, and W. Geyi, "A linear polarization converter with near unity efficiency in microwave regime," *J. Appl. Phys.*, Vol. 121, 144502, 2017.
5. Pfeiffer, C. and A. Grbic, "Millimeter-wave transmitarrays for wavefront and polarization control," *IEEE Trans. Microw. Theory Tech.*, Vol. 61, No. 12, 4407–4417, 2013.
6. Zhao, J. C. and Y. Z. Cheng, 'Ultra-broadband and high-efficiency reflective linear polarization convertor based on planar anisotropic metamaterial in microwave region," *Opt.*, Vol. 136, No. 3, 52–57, 2017.
7. Zheng, Q., C. Guo, G. A. E. Vandenbosch, P. Yuan, and J. Ding, "Dual-broadband highly efficient reflective multi-polarisation converter based on multi-order plasmon resonant metasurface," *IET Microwaves, Antennas Propag.*, Vol. 14, No. 9, 967–972, 2020.
8. Zheng, Q., C. Guo, and J. Ding, "Wideband metasurface-based reflective polarization converter for linear-to-linear and linear-to-circular polarization conversion," *IEEE Antennas Wirel. Propag. Lett.*, Vol. 17, No. 8, 1459–1463, 2018.
9. Grady, N. K., et al., "Terahertz metamaterials for linear polarization conversion and anomalous refraction," *Science*, Vol. 340, No. 6138, 1304–1307, 2013.
10. Pan, W., Q. Chen, Y. Ma, X. Wang, and X. Ren, "Design and analysis of a broadband terahertz polarization converter with significant asymmetric transmission enhancement," *Opt. Commun.*, Vol. 459, 124901, 2020.
11. Ma, X., et al., "An active metamaterial for polarization manipulating," *Adv. Opt. Mater.*, Vol. 2, No. 10, 945–949, 2014.
12. Wang, H. B., Y. J. Cheng, and Z. N. Chen, "Wideband and wide-angle single-layered-substrate linear-to-circular polarization metasurface converter," *IEEE Trans. Antennas Propag.*, Vol. 68, No. 2, 1186–1191, 2020.
13. Doumanis, E., et al., "Electronically reconfigurable liquid crystal based mm-wave polarization converter," *IEEE Trans. Antennas Propag.*, Vol. 62, No. 4, 2302–2307, 2014.
14. Rutz, F., T. Hasek, M. Koch, H. Richter, and U. Ewert, "Terahertz birefringence of liquid crystal polymers," *Appl. Phys. Lett.*, Vol. 89, 221911, 2006.
15. Li, Y., Q. Cao, and Y. Wang, "A wideband multifunctional multilayer switchable linear polarization metasurface," *IEEE Antennas Wirel. Propag. Lett.*, Vol. 17, No. 7, 1314–1318, 2018.
16. Abadi, S. M. A. M. H. and N. Behdad, "Wideband linear-to-circular polarization converters based on miniaturized-element frequency selective surfaces," *IEEE Trans. Antennas Propag.*, Vol. 64, No. 2, 525–534, 2016.
17. Khan, M. I., B. Hu, Y. Chen, N. Ullah, M. J. I. Khan, and A. U. R. Khalid, "Multiband efficient asymmetric transmission with polarization conversion using chiral metasurface," *IEEE Antennas Wirel. Propag. Lett.*, Vol. 19, No. 7, 1137–1141, 2020.
18. Fahad, A. K., et al., "Triband ultrathin polarization converter for X/Ku/Ka-band microwave transmission," *IEEE Microw. Wirel. Components Lett.*, Vol. 30, No. 4, 351–354, 2020.
19. Yang, W., K.-W. Tam, W.-W. Choi, W. Che, and H. T. Hui, "Novel polarization rotation technique based on an artificial magnetic conductor and its application in a low-profile circular polarization antenna," *IEEE Trans. Antennas Propag.*, Vol. 62, No. 12, 6206–6216, 2014.
20. Li, F., et al., "Compact high-efficiency broadband metamaterial polarizing reflector at microwave frequencies," *IEEE Trans. Microw. Theory Tech.*, Vol. 67, No. 2, 606–614, 2019.

21. Jia, Y., Y. Liu, Y. J. Guo, K. Li, and S. Gong, "A dual-patch polarization rotation reflective surface and its application to ultra-wideband RCS reduction," *IEEE Trans. Antennas Propag.*, Vol. 65, No. 6, 3291–3295, 2017.
22. Huang, X., H. Yang, D. Zhang, and Y. Luo, "Ultrathin dual-band metasurface polarization converter," *IEEE Trans. Antennas Propag.*, Vol. 67, No. 7, 4636–4641, 2019.
23. Khan, M. I., B. Hu, Y. Chen, N. Ullah, M. J. I. Khan, and A. R. Khalid, "Multiband efficient asymmetric transmission with polarization conversion using chiral metasurface," *IEEE Antennas Wirel. Propag. Lett.*, Vol. 19, No. 7, 1137–1141, 2020.
24. Bakal, F., A. Yapici, M. Karaaslan, and O. Akgöl, "Microwave absorption performance of hexagonal nano boron nitride doped basalt fabric-reinforced epoxy composites," *Aircr. Eng. Aerosp. Technol.*, Vol. 93, No. 1, 205–211, 2021.
25. Yang, Z., S. Yu, N. Kou, F. Long, Z. Ding, and Z. Zhang, "Ultrathin tri-band reflective cross-polarization artificial electromagnetic metasurface," *Journal of Electromagnetic Waves and Applications*, Vol. 34, No. 10, 1491–1501, 2020.
26. Al-Badri, K. S. L., Y. I. Abdulkarim, F. Ö. Alkurt, and M. Karaaslan, "Simulated and experimental verification of the microwave dual-band metamaterial perfect absorber based on square patch with a 45° diagonal slot structure," *Journal of Electromagnetic Waves and Applications*, 12, 2021.
27. Sağık, M., "Optimizing the gain and directivity of a microstrip antenna with metamaterial structures by using artificial neural network approach," *Wirel. Pers. Commun.*, Vol. 118, No. 1, 109–124, 2021.